
Use of the Gaussian Moment Closure for the Modelling of Continuum and Micron-Scale Flows with Moving Boundaries

J. G. McDonald, J. S. Sachdev, and C. P. T. Groth

University of Toronto Institute for Aerospace Studies, 4925 Dufferin Street,
Toronto, Ontario, Canada, M3H 5T6, mcdonald@utias.utoronto.ca

1 Introduction

Non-equilibrium micron-scale flows, such as those encountered in the complex micron-sized conduits of micro-electromechanical systems and flows associated with chemical-vapour deposition, are difficult to solve using existing mathematical models and numerical methods. In most cases, these flows are in the subsonic to low-supersonic regimes and, due to their micro-geometries, have low Reynolds numbers and remain laminar. Flow Knudsen numbers, Kn , in the range $0.01 < Kn < 10$ may be encountered, even for pressures above one atmosphere, and, as a result, non-continuum and thermal non-equilibrium effects can significantly influence momentum and heat transfer phenomena in typical micro-channel flows [5, 8]. The situation is further complicated by the fact that in many cases, micron-scale flows can involve complex evolving boundaries which require special gridding techniques.

One approach that is showing considerable promise for the treatment of micron-scale flows is moment closures [10]. Moment closures provide an extended set of hyperbolic partial differential equations (PDEs) describing the transport of macroscopic fluid properties. In general, the solution of these PDEs require considerably less effort than obtaining solutions using a particle simulation method. Furthermore, the treatment of non-equilibrium flows with a purely hyperbolic model can have additional advantages from a computational perspective. The hyperbolic moment equations involve only first-order derivatives and can be readily solved using high-order Godunov-type finite-volume schemes coupled with adaptive mesh refinement (AMR) techniques [1, 4, 16]. Schemes of this type are robust, minimize numerical discretization errors, provide accurate resolution of discontinuities, and permit systematic application of physically realistic boundary conditions. When coupled with AMR, they permit treatment of complex and evolving flow geometries and the resolution of highly disparate length scales while, at the same time, optimizing usage of computational resources. They also have narrow

stencils, making them suitable for implementation on massively parallel computers [2, 16]. Note that higher-than-first-order derivatives can be problematic when using adaptive mesh refinement or meshes with embedded boundaries as irregularities in the grid can make accurate evaluation of these derivatives difficult. This situation is avoided with moment closure methods.

2 Gaussian Moment Closure

Levermore [10] has proposed a new hierarchy of non-perturbative moment closures with several desirable mathematical properties. These methods are based on approximate solutions to the Boltzmann equation of kinetic theory and provide a hyperbolic mathematical description of non-equilibrium flows. The lowest-order closure, the 10-moment or Gaussian closure is considered here. It consists of a set of macroscopic transport equations which, in addition to equations for the gas density, ρ , and momentum, ρu_i , contain equations for a symmetric non-equilibrium pressure tensor, P_{ij} . An extension to the standard Gaussian closure for monatomic gases, proposed by Hittinger [9], allows for a treatment of the molecular rotational energy, E_{rot} , present in diatomic gases. This includes a two-time-scale relaxation-time approximation to the collision term. Previous numerical studies indicate that this closure holds considerable promise for describing non-equilibrium transport, at least for subsonic and transonic flows in the slip and transition regimes [11].

For two space dimensions, the Gaussian closure for a diatomic gas can be written in weak conservation form as

$$\frac{\partial \mathbf{U}}{\partial t} + \frac{\partial \mathbf{F}_x}{\partial x} + \frac{\partial \mathbf{F}_y}{\partial y} = \mathbf{S}, \quad (1)$$

where $\mathbf{U} = [\rho, \rho u, \rho v, \rho u^2 + P_{xx}, \rho uv + P_{xy}, \rho v^2 + P_{yy}, P_{zz}, E_{\text{rot}}]^T$ is the vector of conserved variables, \mathbf{F}_x and \mathbf{F}_y are x - and y -direction components of the flux dyad $\vec{\mathbf{F}}$, and \mathbf{S} is the source vector.

3 Parallel AMR Solution Scheme

A Godunov-type, finite-volume scheme has been developed for the solution of the two-dimensional weak conservation form of the Gaussian moment equations as given in Eq. 1, on multi-block quadrilateral meshes. The scheme allows for solution-directed block-based AMR and an efficient and highly scalable parallel implementation has been achieved via domain decomposition. An arbitrary Lagrangian Eulerian (ALE) treatment is used to describe situations with moving boundaries. The ordinary differential equation resulting from spacial discretization procedure that governs the evolution of the average solution in a computational cell of the multi-block mesh, $\bar{\mathbf{U}}$, is given by

$$\frac{d\bar{\mathbf{U}}}{dt} = -\frac{1}{A} \sum_k \left[\vec{\mathbf{F}}_k - \vec{w}_k \mathbf{U}_k \right] \cdot \hat{n}_k \Delta \ell_k - \frac{\bar{\mathbf{U}}}{A} \frac{dA}{dt} + \mathbf{S}, \quad (2)$$

where A is the cell area, \vec{w} , \hat{n}_k and $\Delta\ell_k$ are the velocity of, unit normal to, and length of the k^{th} cell face, while $\vec{\mathbf{F}}_k$ and \mathbf{U}_k are the flux dyad and solution state at the quadrature point on the k^{th} face. Second-order spacial accuracy is achieved via limited linear reconstruction. Flux evaluations are carried out using Roe's approximate Riemann solver [14]. Mesh refinement is carried out according to physics-based refinement criteria as well as to resolve embedded/moving boundaries. Refer to the recent paper by McDonald and Groth [11] for further details of the parallel AMR scheme.

4 Mesh Adjustment Algorithm

Implementation of the preceding finite-volume scheme with the mesh adjustment scheme proposed recently by Sachdev and Groth [15] is now considered. The mesh adjustment scheme provides an automated treatment for fixed and moving, non-grid-aligned boundaries embedded in a body-fitted, multi-block mesh. Similar in nature to the Cartesian-cut-cell methods developed by Bayyuk *et al.* [3] and Murman *et al.* [12], this scheme allows for the nodes of an underlying body-fitted mesh to be adjusted so as to coincide with the embedded boundary. By making only local alterations to the grid, this scheme enables the solution of unsteady flows involving moving boundaries or for steady flow problems involving stationary boundaries that are not necessarily aligned with the mesh, while preserving the structured nature of the blocks and avoiding the creation of small cut cells that are often generated by traditional cut-cell approaches. In addition, the mesh adjustment algorithm is fully compatible with block-based AMR and parallel implementation via domain decomposition used in the finite-volume solution scheme.

Mesh adjustment is carried out in several steps. Firstly, a pre-mesh-adjustment flagging is used in order to determine which cells may require adjustment. The first mesh-adjustment step involves identifying sharp corners on the interfaces. The cells flagged for adjustment which contain each sharp corner are identified and their nearest nodes moved to the corners. For the remaining cells tagged for adjustment, the nodes which are closest to the boundary are moved to the point of intersection between the interface and the mesh lines, this can be seen in Figure 1(b). This movement will leave cells that are bisected diagonally by the boundary. A secondary adjustment step is used to move the nearest node of bisected cells so that it also lies on the boundary. This step will produce triangular cells, as seen in Figure 1(c); these cells are simply treated as degenerate quadrilaterals with two coincident nodes. The final step in the mesh-adjustment algorithm involves use of a ray-tracing technique to determine which of the cells are within the flow domain and which are outside the flow domain. The resulting mesh remains structured and does not have neighbouring cells of radically different size. The present implementation also allows for moving embedded boundaries whose motion can be prescribed either explicitly or through a level-set method [13].

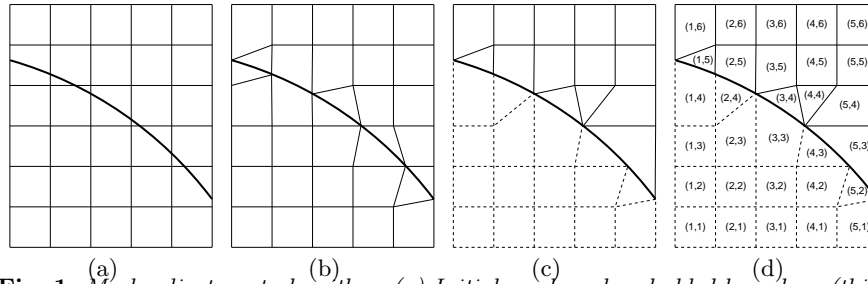


Fig. 1. Mesh adjustment algorithm: (a) Initial mesh and embedded boundary (thick line), (b) result of primary adjustment, (c) result of secondary adjustment (dashed lines indicate inactive cells), and (d) example of (i, j) -indexing on an adjusted mesh.

5 Numerical Results

Several flow problems are now considered. The first such problem is subsonic boundary-layer flow over a flat plate. The goal in this case is to demonstrate that the embedded boundary treatment and hyperbolic nature of the governing equations will yield smooth predictions of the frictional forces acting on the plate; traditional cut-cell-type approaches combined with the Navier-Stokes equations have been shown to produce large oscillations in viscous drag predictions [6]. Next, subsonic flow past a circular cylinder is considered. This case is considered to illustrate the scheme's applicability to transition-regime flows. Previous investigation using body-fitted meshes has shown good agreement with experimental results [11] and it will be shown that equally good results can be achieved with embedded boundary treatment. Finally, a channel flow with complex moving geometry is considered to illustrate the potential of the proposed approach for tackling such problems.

Subsonic boundary-layer flow past a flat plate is considered. For the case of interest, the free-stream Mach number is 0.2 and Reynolds number per unit length is 2000. For this situation, the Knudsen number was 1.5×10^{-4} , which indicates that the flow is in the continuum regime. Two computational meshes are considered: one aligned with, or at 0° to, the plate and a second mesh at 30° to the plate. Both meshes initially consisted of one 16×16 Cartesian square block. This block was then subjected to six or eight mesh refinements such that at each level of refinement, any block crossed by the boundary was refined. Sections of the resulting meshes are shown in Figure 2.

Numerical predictions of the friction coefficient, C_f , are shown in Figure 3. In the figure, comparisons are made to the classical boundary layer results of Blasius. It can be seen that there is good agreement between the computed results and Blasius' solution. There are no oscillations present in the predicted skin friction coefficients, even when the flat plate intersects the grid at an angle. Furthermore, on the more refined mesh with eight levels of refinement, the numerical solutions are nearly indistinguishable from the Blasius solution.

As a second case, subsonic flow past an circular cylinder is considered. Experimental measurements of drag on the cylinder have been obtained by

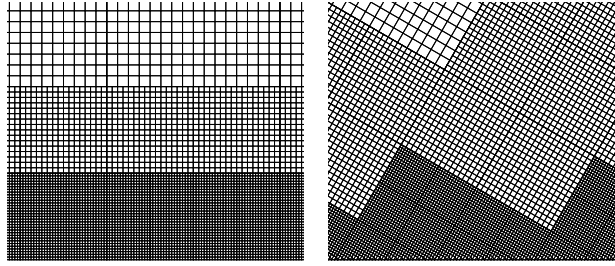


Fig. 2. (left) Section of 48128-cell mesh with flat plate embedded at 0° . (right) Section of 65024-cell mesh with flat plate embedded at 30° .

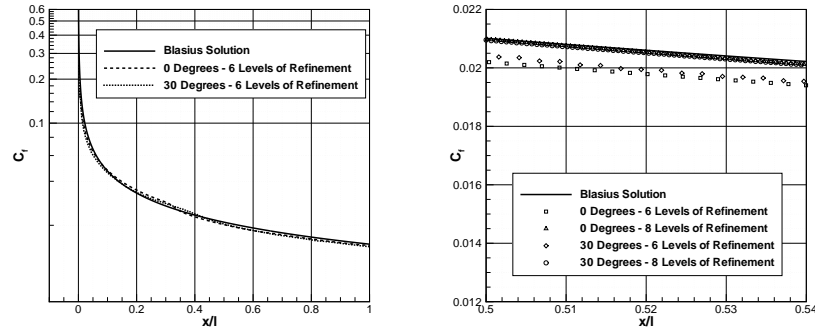


Fig. 3. Coefficient of friction calculated for a Cartesian grid with an embedded flat plate at 0° and 30° to the grid as compared to Blasius solution.

Coudeville *et al.* [7]. The Gaussian closure has previously been applied to this case using body fitted meshes [11] for several speed ratios, S , and a wide range of Knudsen numbers in the continuum and transition regimes. These predictions are shown in Figure 4, where numerical results are compared to experimental data of Coudeville and an analytical expression of Paterson [11].

In order to demonstrate that the present embedded mesh treatment can recover these previous results with virtually equal accuracy, values for the coefficient of drag were computed for varying Knudsen numbers for flow with a speed ratio of 0.107. Predicted results obtained using the adjusted mesh scheme are compared in Figure 4 with the Gaussian-closure solutions obtained using a body fitted mesh, as well as to the experimental results. Clearly, the agreement between body-fitted and non-aligned-mesh results is excellent.

Coirier explored Mach 0.1 flow through a branched channel containing fourteen pin cooling fins [6]. A similar geometry has been considered here for both continuum and non-equilibrium flow, except two rows of the pins are now assumed to oscillate with a prescribed motion. The results of the continuum situation can be seen in Figure 5.

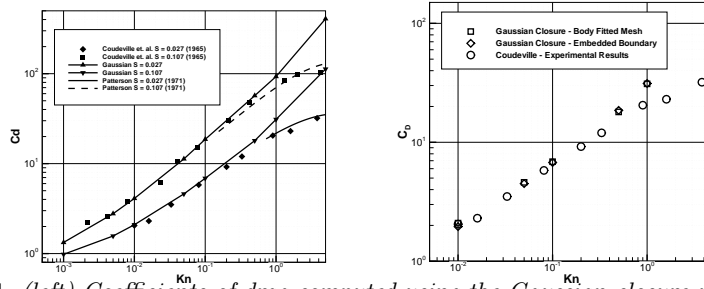


Fig. 4. (left) Coefficients of drag computed using the Gaussian closure with a body-fitted mesh compared with experimental data and an approximate solution due to Paterson. (right) Coefficients of drag computed using the Gaussian closure with a body-fitted mesh and a Cartesian mesh with an embedded boundary at a speed ratio of 0.107 are compared with experimental data.

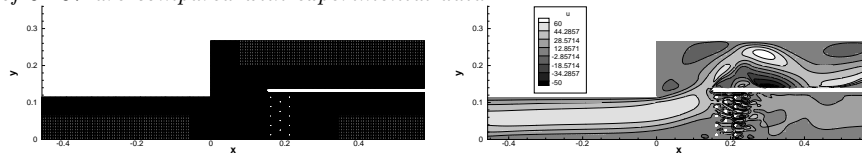


Fig. 5. Computational grid and x -direction velocity contours for flow through a branched channel with moving pins.

6 Conclusions

The use of the Gaussian moment closures with embedded-mesh treatment for continuum- and transition-regime flows has been demonstrated. The proposed algorithm allows for accurate treatment of micron-scale flows with embedded and possible moving boundaries, not aligned with the mesh.

References

1. M. J. Aftosmis, M. J. Berger, and J. E. Melton. *AIAA J.*, 36(6):952–960, 1998.
2. M. J. Aftosmis, M. J. Berger, S. M. Murman. Paper 2004-1232, AIAA, 2004.
3. S. A. Bayyuk, K. G. Powell, and B. van Leer. Paper 93-3391, AIAA, 1993.
4. M. J. Berger and P. Colella. *J. Comput. Phys.*, 82:67–84, 1989.
5. A. Beskok, G. E. Karniadakis. *J. Thermophys. Heat Transfer*, 8(4):647, 1994.
6. W. J. Coirier. PhD thesis, University of Michigan, 1994.
7. H. Coudeville, P. Trepaud, E.A. Brun. *Proceedings of the Fourth International Symposium on Rarefied Gas Dynamics*, New York, 1965. Academic Press.
8. J. C. Harley, Y. Huang, H. B. Bau, J. N. Zemel. *J. Fluid Mech.*, 284:257, 1995.
9. J. A. Hittinger. PhD thesis, University of Michigan, 2000.
10. C. D. Levermore. *J. Stat. Phys.*, 83:1021–1065, 1996.
11. J. McDonald and C.P.T. Groth. Paper 2005-5035, AIAA, June 2005.
12. S. M. Murman, M. J. Aftosmis, M. J. Berger. Paper 03-1119, AIAA, 2003.
13. S. Osher and J. A. Sethian. *J. Comput. Phys.*, 79:12–49, 1988.
14. P. L. Roe. *J. Comput. Phys.*, 43:357–372, 1981.
15. J. S. Sachdev and C. P. T. Groth. *Proceedings of the 3rd International Conference on Computational Fluid Dynamics*, 109–115, 2004.
16. J. S. Sachdev, C. P. T. Groth, and J. J. Gottlieb. *Int. J. CFD*, 19(2):157, 2005.